Astron. Astrophys. 284, 810–826 (1994)

ASTRONOMY AND ASTROPHYSICS

A new UBV and proper motion survey in the anticentre direction at intermediate galactic latitude: kinematics of the Galaxy's stellar populations*

D.K. Ojha[1], O. Bienaymé[1], A.C. Robin[1,2], and V. Mohan[3]

[1] Observatoire de Besançon, 41 bis, Av de l'Observatoire, BP1615, F-25010 Besançon Cedex, France
[2] Observatoire de Strasbourg, CNRS URA 1280, 11 rue de l'Université, F-67000 Strasbourg, France
[3] Uttar Pradesh State Observatory, Manora Peak, Nainital, 263129, India

Received 13 September 1993 / Accepted 15 October 1993

Abstract. We present the results from a new complete absolute proper motion survey in the direction of intermediate galactic latitude (l = 167.5°, b = 47.4°) with respect to background galaxies and quasars, using a set of Tautenburg and OCA (Observatoire de la Côte d'Azur) Schmidt plates, obtained at different epochs separated by ~25 years. Photometric U, B and V survey has been done for 4167 objects covering 18.8 square degree field and proper motions have been calculated for 1888 objects for a 8.6 deg^2 area. The resulting catalogues are complete down to V=17, B=19 and U=16.5. An average proper motion accuracy of 0."25 per century was achieved for stars brighter than V=16, with the uncertainties increasing to ~ 0."4 per century at V>16. The photometric accuracy ranges between 0.07 to 0.10 in the three bands.

We utilize our photometric and absolute proper motions data to investigate the structure and kinematics of the Galaxy. We have determined ultraviolet excesses and distances for a subsample of 2685 stars in the color range 0.3≤(B-V)≤0.9 and with V≤17. Thus we have been able to probe the kinematical distribution of F and G– type stars to distances up to 3.5 kpc from the plane. We obtain a value -0.21±0.1 kpc^{-1} for the galactic radial gradient of velocity dispersion ($\partial ln\sigma^2_{U+W}/\partial r$). By comparing the ratio of stars in this direction to the number of stars towards galactic centre at intermediate latitude (l = 3°, b = 47°), give a strong evidence that the scale length of old disk is rather short (2–2.5 kpc). Because of the kinematical biases inherent in our data sample, we can not present definite kinematical parameters for the intermediate population, but reasonable estimates would be an asymmetric drift of 57±4 km s^{-1} and velocity dispersion (σ_V) of 60±3 km s^{-1} at a mean distance (above the plane) of z = 2 kpc.

Key words: astrometry – reference systems – Galaxy: kinematics and dynamics – Galaxy: stellar content – Galaxy: structure

1. Introduction

During the past decade galactic structure studies concentrated on star counts, adjusting models of the Galaxy to match the observed number-magnitude-color distributions, and setting constraints on the parameters of the stellar population models (Bahcall & Soneira 1981; Gilmore & Wyse 1985; Robin & Crézé 1986; Bienaymé et al. 1987). Now it has become apparent that we require an additional observable parameter to constrain further the galactic model parameters and to describe the set of star counts with reasonable accuracy. Proper motion surveys offer a means for a detailed investigation of the kinematics of our Galaxy. It is only recently that proper motion surveys to faint magnitudes were carried out by various authors in different directions e.g. Chiu (1980), Reid (1990), Spaenhauer (1989), Majewski (1992), Bienaymé et al. (1992), Soubiran (1992a,b) and Reid & Majewski (1993) with good accuracy. These measurements include both photometry and proper motions.

One may gain kinematical information about a star from either radial velocities or proper motions. One advantage of the latter is that two-dimensional information is obtained, so that with an appropriate selection of fields (say the galactic centre and the anticentre), three-dimensional structure (the shape and size of the velocity fields) can be more efficiently deduced. Finally, there must be some way to estimate distances, so that the proper motions may be converted to velocities, and the entire survey placed within a structural context. Here we utilize these

Send offprint requests to: D.K.Ojha

* Based on observations made at Nainital(India), OHP(France), on photographic plates obtained with the OCA and Tautenburg Schmidt telescopes. Digitizations made with the MAMA measuring machine. MAMA is developed and operated by INSU (Institut National des Sciences de l'Univers).

new UBV and proper motions data in order to address problems of galactic structure and kinematics.

Here we present the results of an absolute proper motion study in the direction (l = 167.5°, b = 47.4° ; $\alpha_{1950} = 09^h38^m$, δ_{1950} = +50°08′) for a 8.6 square degree field as part of an investigation of galactic structure and evolution. The proper motion program is based on MAMA measurements and the absolute proper motion was calculated with respect to reference galaxies and quasars. The error in the proper motions is given for each star. The overall proper motion accuracy turns out to be better than 0."3 per century. Schilbach (1993) had described the comparison of our astrometric results by using two different methods for the same field.

The first part of this paper explains the details of our data reduction methods. In Sect. 2 we discuss specifically the photographic plate data used in this survey. The path from instrumental photographic photometry to final magnitudes is explained in Sect. 3. In Sect. 4 we explain in detail our astrometric techniques. This includes a section describing the derivation of absolute proper motions and the overall accuracy of the proper motion survey. In Sect. 5 we discuss the comparison of our photometric and proper motions data with other data sets as well as with Besançon model predictions. The mainsprings of Besançon population synthesis model are described in Robin & Crézé (1986) (star formation, stellar evolution, photometric predictions), Bienaymé et al. (1987) (dynamical consistency), Robin & Oblak (1987) (kinematic predictions). This model can predict without additional empirical ingredients the multivariate distribution of astrometric and photometric observables. We then proceed to transform our proper motions into space velocities. We also address the possible introduction of systematic errors on distance measurement.

2. Plate material

The photographic material used in this survey is described in Table 1. All plates used were taken from Tautenburg and OCA Schmidt telescopes between 1967 and 1993. The plates were measured with the MAMA measuring machine in its scanning mode (Guibert 1983; Berger et al. 1991). Plates measured for astrometric purposes are digitized with a 10 μm pixel. Digitized images are processed on line for star detection and centering. A total of 11 Schmidt plates (1967-1992) have been used for the astrometric reduction, giving a time base of $\sim$ 25 years.

For the U, B and V photometry 6 OCA plates were used, which were also digitized with a 10 μm pixel. The filter/emission combinations of the 6 OCA plates give a system close to the Johnson U, B and V bands.

Our final photometric survey covers 8761 objects in B & V magnitudes and 4167 objects in U,B & V magnitudes covering 18.8 square degree field. The proper motion catalogue having U,B & V magnitudes contains 1888 objects while 3872 objects have only B & V magnitudes in a 8.6 square degree area. The catalogues are complete down to V=17, B=19 and U=16.5.

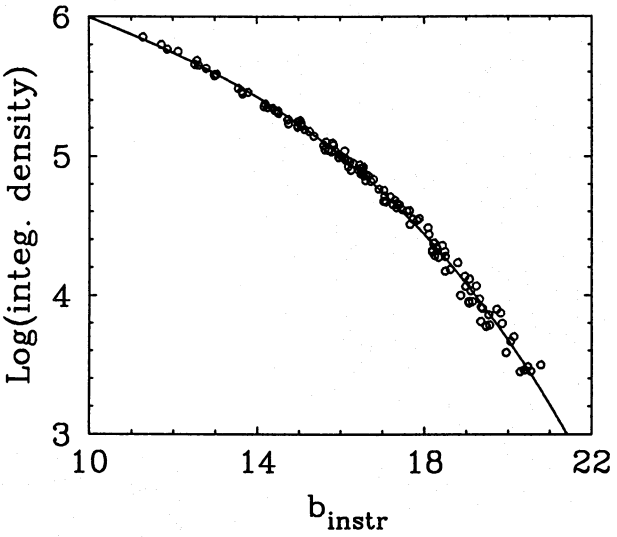

Fig. 1. Calibration curve (Instrumental magnitudes versus logarithm of the integrated density on plates) for OCA plate 2812. In total 138 standards were used. The dispersion is 0.08 mag

3. Photographic photometry

3.1. Calibration curve

Two kinds of photometric sequences have been used to calibrate the plates. First UBV CCD photometry (Mohan et al. 1993) have been obtained with the 1 m telescope of the Uttar Pradesh State Observatory at Nainital (India) and 1.2 m telescope of Observatoire de Haute-Provence (OHP) in France on 19 different nights during January 1991 to January 1993. Second photoelectric sequences from Notni et al. (1979) in the same field were used to complete the set of standards. A total of $\sim$ 150 standards in U, B and V magnitudes well distributed on OCA plates were used in the calibration. U, B and V standard colors were converted into photographic instrumental colors (u,b,v) using Eqs. (1) – (3).

$$v_{inst} = V_{Johnson} - 0.138(B-V) + 0.006(U-B) \quad (1)$$

$$b_{inst} = B_{Johnson} - 0.162(B-V) - 0.048(U-B) \quad (2)$$

$$u_{inst} = U_{Johnson} - 0.155(B-V) + 0.096(U-B) \quad (3)$$

These equations have been previously determined by Mohan & Crézé (1987) for OCA Schmidt telescope. Calibration curves were obtained by fitting a third degree polynomial to the logarithm of integrated density versus magnitudes plot. The calibration curve for OCA plate 2812 is shown in Fig. 1. The photographic magnitudes of the detected object have been calculated by inverting the Eqs. (1) – (3). For all plates the rms magnitude scatter ranges between 0.06 to 0.10 in the magnitude range 10 to 18. The plate to plate dispersion in all magnitude range is shown in Table 2.

Residuals from the best fit polynomial calibration are plotted in Fig. 2 as a function of color for 65 standards brighter than V = 16. As can be seen from the figure, there is no significant

Table 1. Plate material

Plate number	Emulsion+ filter	Color	Exposure time(min)	Epoch	Scale ("/mm)
Tautenburg Schmidt plates					
2410	Astro-Spezial+GG13	B	60	04/03/1967	51.40
2414	Astro-Spezial+GG13	B	60	06/03/1967	51.40
2415	Astro-Spezial+GG13	B	60	06/03/1967	51.40
2416	Astro-Spezial+GG13	B	60	06/03/1967	51.40
2420	Kodak 103a-G+GG11	V	45	07/03/1967	51.40
2430	Kodak 103a-G+GG11	V	45	08/03/1967	51.40
6568	ZU-21+GG13	B	28	25/11/1987	51.40
6569	ZU-21+GG13	B	27	25/11/1987	51.40
OCA Schmidt plates					
2787	IIaO+UGI	U	85	02/01/1992	65.25
2790	IIaD+GG495	V	64	02/01/1992	65.25
2809	IIaO+GG385	B	60	02/02/1992	65.25
2812	IIaO+GG385	B	60	03/02/1992	65.25
2986	IIaD+GG495	V	60	17/01/1993	65.25
3003	IIaO+UGI	U	61	12/02/1993	65.25

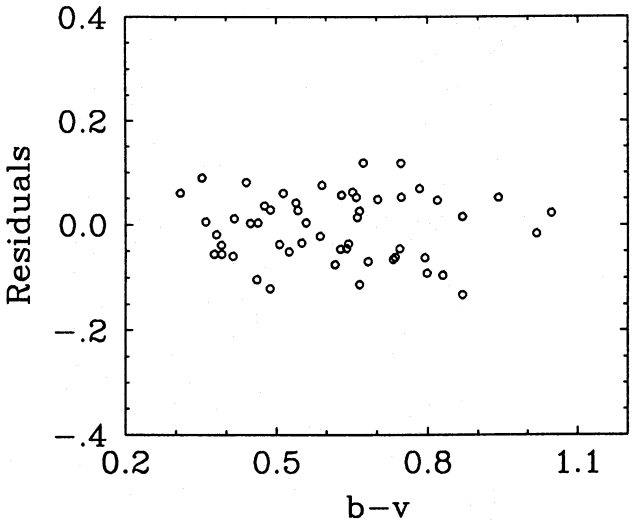

Fig. 2. Residuals of the standards to the calibration curve versus instrumental $b - v$ color (for stars with V<16)

color effect. The plate to plate magnitude comparison shows geometrical variations (the variation of the instrumental response as a function of the position in the field). To look into this problem, we have sufficient bright standards well distributed over all the plates. Using a linear fit in X and Y coordinates (Mohan & Crézé 1987), we have determined geometrical coefficients for the plate in each color. These corrections have been applied in V, B & U magnitudes for all stars. The U-B versus B-V diagrams without geometrical correction and after geometrical correction are shown in Fig. 3a and b. The dispersion is lowered after applying the correction. The correction confines the data along the main sequence.

For the homogeneity of the photometric sample, it is important to separate resolved objects (e.g. galaxies, blends, etc.) from unresolved ones (e.g. stars). To classify objects as stars or

Table 2. rms. scatter of magnitudes from plate to plate comparison

B range	σ_V	σ_B	σ_U
11-12	0.06	0.05	0.07
12-13	0.06	0.05	0.07
13-14	0.07	0.06	0.08
14-15	0.07	0.06	0.08
15-16	0.07	0.06	0.08
16-17	0.08	0.06	0.08
17-18	0.08	0.07	0.09

galaxies, the logarithm of MAMA density flux over object area is plotted in Fig. 4. Galaxies have a lower surface brightness and hence a lower density flux for a given area. A higher-order polynomial (e.g. order 15 in this case) was derived in an iterative procedure with stepwise exclusion of objects with large residuals. The resulting function was accepted as the stellar one. The galaxies are then considered to be all the objects below this curve. The reliability of the classification decreases rapidly for stars closer to the limiting magnitude of the plate. However the separation looks good for stars having logarithm of density $\geq$ 4.2 ($m_v \sim 18$). The deepest plate (T2415) has been used for this purpose. To test our classification further, we have compared our star counts (see Sect. 5) with predictions of Besançon stellar population model and also with other surveys. There is good agreement of star counts in the V band between the model and the observations for 12<V<17 (see Sect. 5.2).

3.2. Completeness

Histogram of standard V magnitude counts from two OCA plates is shown in Fig. 5. V counts appear to be complete at V=17. From similar histogram, the completeness limits of the B and U counts are found to be B=19 and U=16.5.

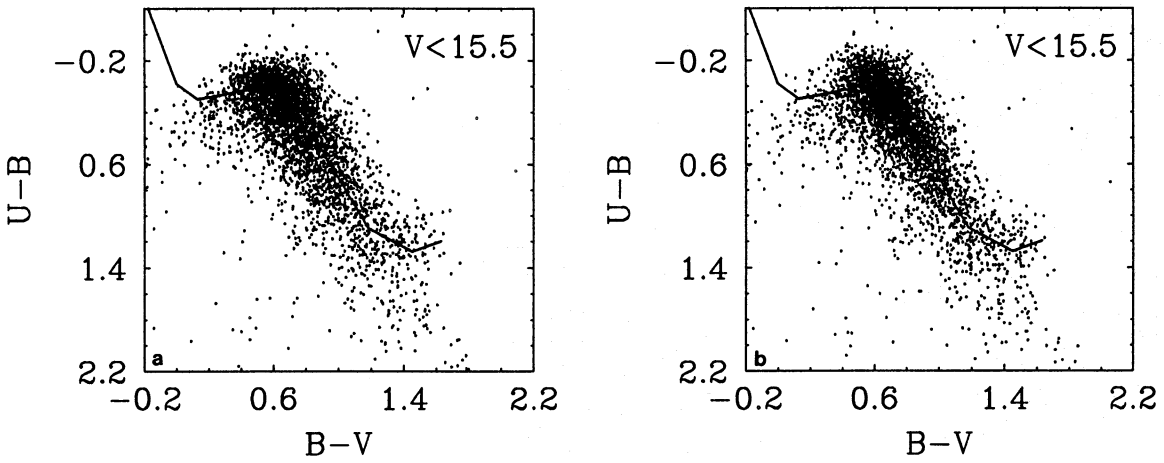

Fig. 3a and b. U-B versus B-V diagram without geometrical correction and after geometrical correction. The full line locates the main sequence

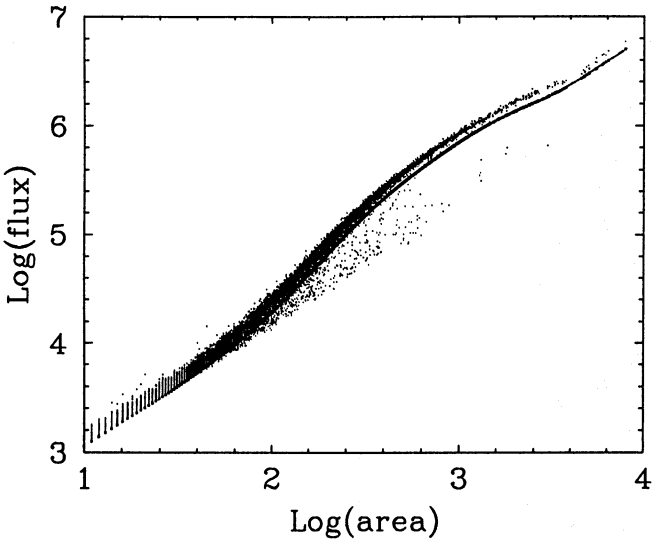

Fig. 4. MAMA density flux over object area. The line represents the distance of 1 σ from the "stellar curve"

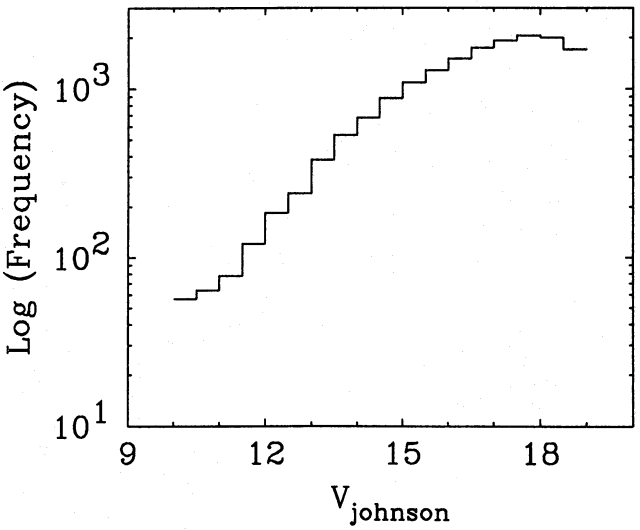

Fig. 5. Histogram of the V star counts. The completeness limit is V = 17

4. Astrometry

As a first step the astrometric analysis has been conceived as purely differential. In a second step the relative proper motions have been shifted to absolute proper motions using the extragalactic objects in the field. The displacement of each stellar image is measured relative to the framework defined by all stars in the field. The overall error results from the inaccuracies from the centering process, plate to plate transformations and systematic effects such as color effects or magnitude effects.

4.1. Cross-identification

Using a few bright stars, a first approximate plate to plate transformations are computed between the reference and other plates. The centre from one plate is transformed into the coordinate system of the other one and counterpart candidates are searched for within a 40 μm radius (2.5 arcseconds for OCA plate) around each projected centre. The calculation is iterative and rejects stars giving large residuals in position. The best plate in terms of image quality and depth has to be chosen as the reference plate. The individual paired data sets are then merged to give one image list for each epoch.

4.2. Plate transform

A mathematical transform is used to model the transformation between plate coordinates from the two epochs. The mathematical transformations used are orthogonal functions

$$X = f_x(x,y) = \sum_{n,m}^{N,N} \alpha_{n,m} P_{n,m}(x,y)$$

$$Y = f_y(x,y) = \sum_{n,m}^{N,N} \beta_{n,m} P_{n,m}(x,y)$$

Table 3. Plate to reference plate (T2415) transforms

Plate No.	Number of common stars	Number of reference stars	Total time elapsed (years)
T2410	9624	2026	-0.005
T2414	11450	2075	0.000
T2416	7401	1281	0.000
T2420	10716	1776	0.182
T2430	11848	2049	0.185
T6568	12314	2079	20.724
T6569	12034	2073	20.724
Cer2790	9166	2224	24.742
Cer2809	10859	2223	24.827
Cer2812	10417	2136	24.830

Where (x, y) represent the observed coordinates of the star on one of the compared plate and (X, Y) are the coordinates of the same star after transformation refered to the system of reference plate. $P_{n,m}(x, y)$ is a polynomial in x & y of order n and N is the order chosen for the transformation. The advantage of using orthogonal polynomial instead of ordinary polynomial is that the determination of the error of each coefficient is independent of the other and there is no more correlation between the evaluated coefficients of the orthogonal model. The set of polynomials depends on the exact distribution of reference stars. For a uniform distribution of reference stars over a rectangular area, the combination of the orthogonal polynomial would be nearly similar to Legendre polynomial. The problem is to compute the set of $\alpha_{n,m}$ and $\beta_{n,m}$ coefficients for $n = 0, \ldots, N$ and $m = 0, \ldots, N$ which minimizes

$$\sigma_x^2 = \sum_{i=1}^{Ns} (X_i - x_{0i})^2$$

$$\sigma_y^2 = \sum_{i=1}^{Ns} (Y_i - y_{0i})^2$$

Where Ns is the total number of stars used in the transformation and (x_{0i}, y_{0i}) are the observed coordinates of stars on the reference plate.

We have selected overall 2000 stars brighter than $m_v = 17$ to compute the mathematical transformation. The large number of stars allow to compute high order tranformation with a good global accuracy and to model distortion of small size. Order 4 or 6 for $P_{n,m}(x, y)$ (respectively 15 or 28 $\alpha_{n,m}$ or $\beta_{n,m}$ coefficients) gives the best fit with a position error of less than 0.2 μm. Similar method has been presented by Chareton et al. (1993). The accuracy of the computed transform is given by a function in (x, y) called "transform error" (Bienaymé 1993). The transform error value increases with the order of the polynomial expansion and is largest along the edge of the field. Figure 6a and b show the isolevels of transform error for 4th and 10th order transform between two Tautenburg Schmidt plates e.g. T2415 & T2414 respectively. In the central part accuracy is 0.2 μm. Since the number of stars defining the reference system used are in high density, the transform error keeps low values even with the large number of coefficients. However due to the high order used, the transform is badly defined along the edge of the plate. Also due to very few stars at the corner of the plate, the transform error keeps high values. By using high order transform, we expect to detect distortions with a lower accuracy. Figure 6c and d show the difference between 10th and 4th order x and y tranforms . The amplitude of differences is about 0.8 μm, which is of the order of the accuracy of the 10th order transform. We expect that such differences can model small scale distortions, but due to their small amplitudes below 0.8 μm they are not significantly modelled by the 10th order transform. Finally we do not find any significant distortions with amplitude larger than 0.8 μm. So very high order transforms are unnecessary. For our final astrometric reduction, the order of the transform has been chosen to be 4. Table 3 indicates the results of cross-identification of all plates compared with the reference plate 2415, the elapsed time since the date of the reference plate, the number of common objects after cross-identification and the number of objects used in the transformation.

4.3. Proper motion determination

For each plate $k = 1, \ldots, K$ and for each star $i = 1, \ldots$,Ns we have transformed coordinates (X_{ki}, Y_{ki}) in reference system defined by the reference plate and the displacement between transformed coordinates and reference coordinates

$$\Delta x_{ki} = X_{ki} - x_{0i}$$

$$\Delta y_{ki} = Y_{ki} - y_{0i}$$

Proper motions are given by

$$X_{ki} = x_{0i} + \Delta x_{ki} = X_{0i} + \mu_i^x t_k + \epsilon_{ki}^x$$

$$Y_{ki} = y_{0i} + \Delta y_{ki} = Y_{0i} + \mu_i^y t_k + \epsilon_{ki}^y$$

It happens that the proper motion measurements are degraded because of blended images on one of the plates. To solve this problem, a weighting matrix for each star and each coordinate (w_{ki}^x, w_{ki}^y) has been introduced. Here the determination of proper motion is a least square problem consisting of determining the position of star i at initial epoch $\begin{pmatrix} X_{0i} \\ Y_{0i} \end{pmatrix}$, and its proper motion $\begin{pmatrix} \mu_i^x \\ \mu_i^y \end{pmatrix}$ which minimize $\begin{pmatrix} \epsilon_{ki}^x \\ \epsilon_{ki}^y \end{pmatrix}$. The solution is obtained by inverting the 2×2 matrix of the normal equations (see Soubiran 1992a) which are given by

$$\begin{pmatrix} \sum w_{ki}^x & \sum t_k w_{ki}^x \\ \sum t_k w_{ki}^x & \sum t_k^2 w_{ki}^x \end{pmatrix} \begin{pmatrix} X_{0i} \\ \mu_i^x \end{pmatrix} = \begin{pmatrix} \sum X_{ki} w_{ki}^x \\ \sum X_{ki} t_k w_{ki}^x \end{pmatrix}$$

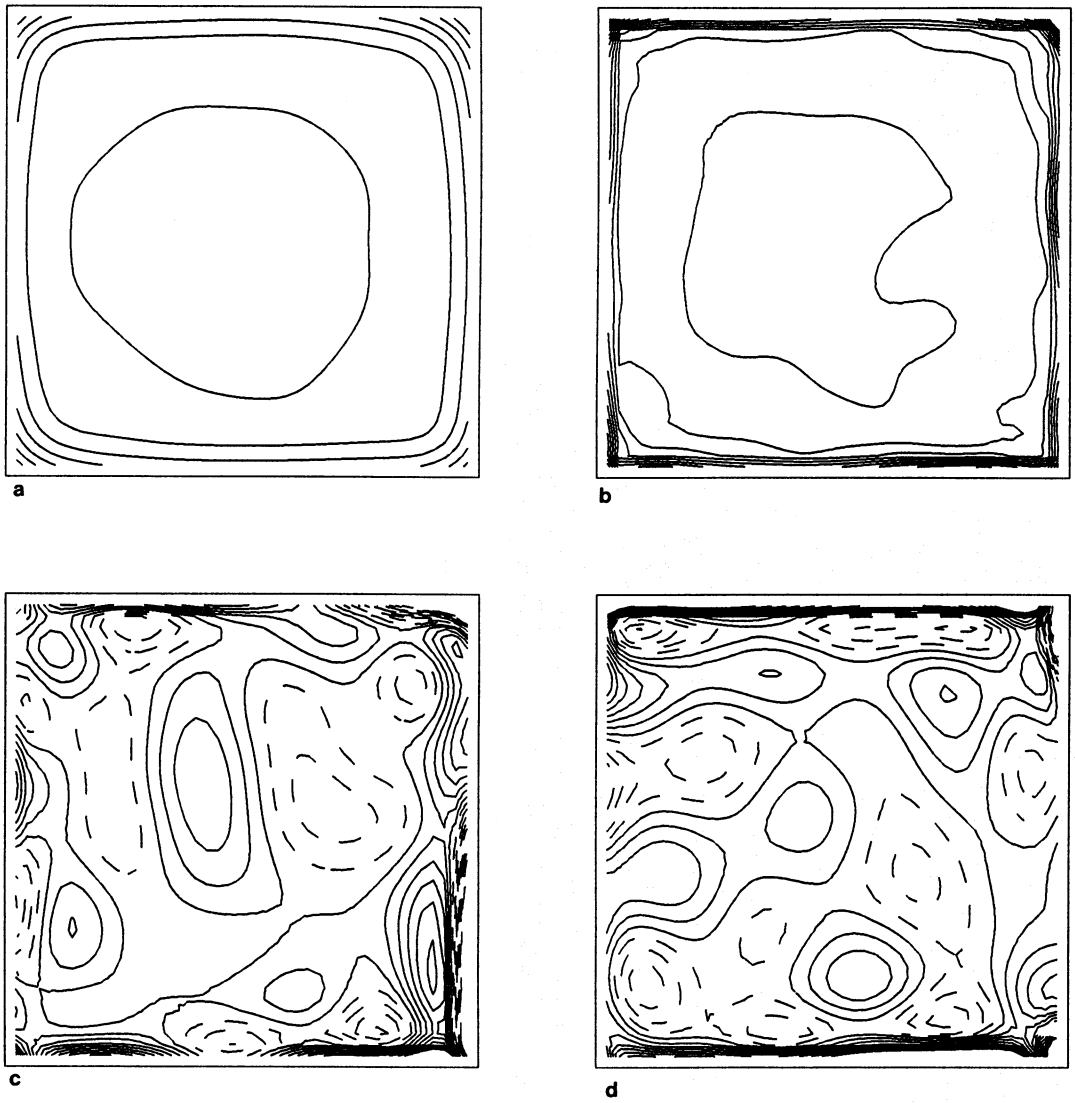

Fig. 6. a Isocontours of the transform error for 4th order transform. Distance between isocontours is 0.05 micron. Inner isocontour is 0.1 micron level. **b** Isocontours for 10th order transform. Distance between isocontours is 0.1 micron. Inner isocontour is 0.2 micron level. **c** and **d** Isocontours of the difference between 10th and 4th order X and Y tranform. Step between isocontour is 0.2 micron in both case. The first dashed line gives zero level

and

$$\begin{pmatrix} \sum w_{ki}^y & \sum t_k w_{ki}^y \\ \sum t_k w_{ki}^y & \sum t_k^2 w_{ki}^y \end{pmatrix} \begin{pmatrix} Y_{0i} \\ \mu_i^y \end{pmatrix} = \begin{pmatrix} \sum Y_{ki} w_{ki}^y \\ \sum Y_{ki} t_k w_{ki}^y \end{pmatrix}$$

In our case we have used the weighting matrix

$$w = \frac{1}{\sigma_c^2 + \sigma_t^2} \quad (\sigma_t \ll \sigma_c)$$

which is a combination of σ's from centering and transformation processes respectively. Here σ_c depends on magnitude and σ_t depends on the star position on the plate. In order to estimate the accuracy of the centering methods, we have plotted the residuals in x and y coordinates against V magnitude (Figs. 7a-d) for reference plate (T2415) and one of the OCA plate (Cer 2809). Figure 7a and b shows the dispersion mainly resulting from the centering of the stars (because for the reference plate T2415, the contribution of proper motion is null). Standard deviations in μm of centering methods as a function of magnitude is given in Table 4. Overall dispersion in reference plate T2415 ranges from 0.7 μm at magnitude 11 to 2.2 μm at magnitude 17. The errors in proper motions are derived from the matrix of variance and covariance given by Pelat (1988) as

$$V \begin{pmatrix} x \\ \mu^x \end{pmatrix} = \frac{\sigma_x^2}{\sum (w_k^x t_k - \bar{t})^2} \begin{pmatrix} \sum \frac{1}{w_k^x} \sum w_k^x t_k^2 & -\bar{t} \\ -\bar{t} & 1 \end{pmatrix}$$

and

$$V \begin{pmatrix} y \\ \mu^y \end{pmatrix} = \frac{\sigma_y^2}{\sum (w_k^y t_k - \bar{t})^2} \begin{pmatrix} \sum \frac{1}{w_k^y} \sum w_k^y t_k^2 & -\bar{t} \\ -\bar{t} & 1 \end{pmatrix}$$

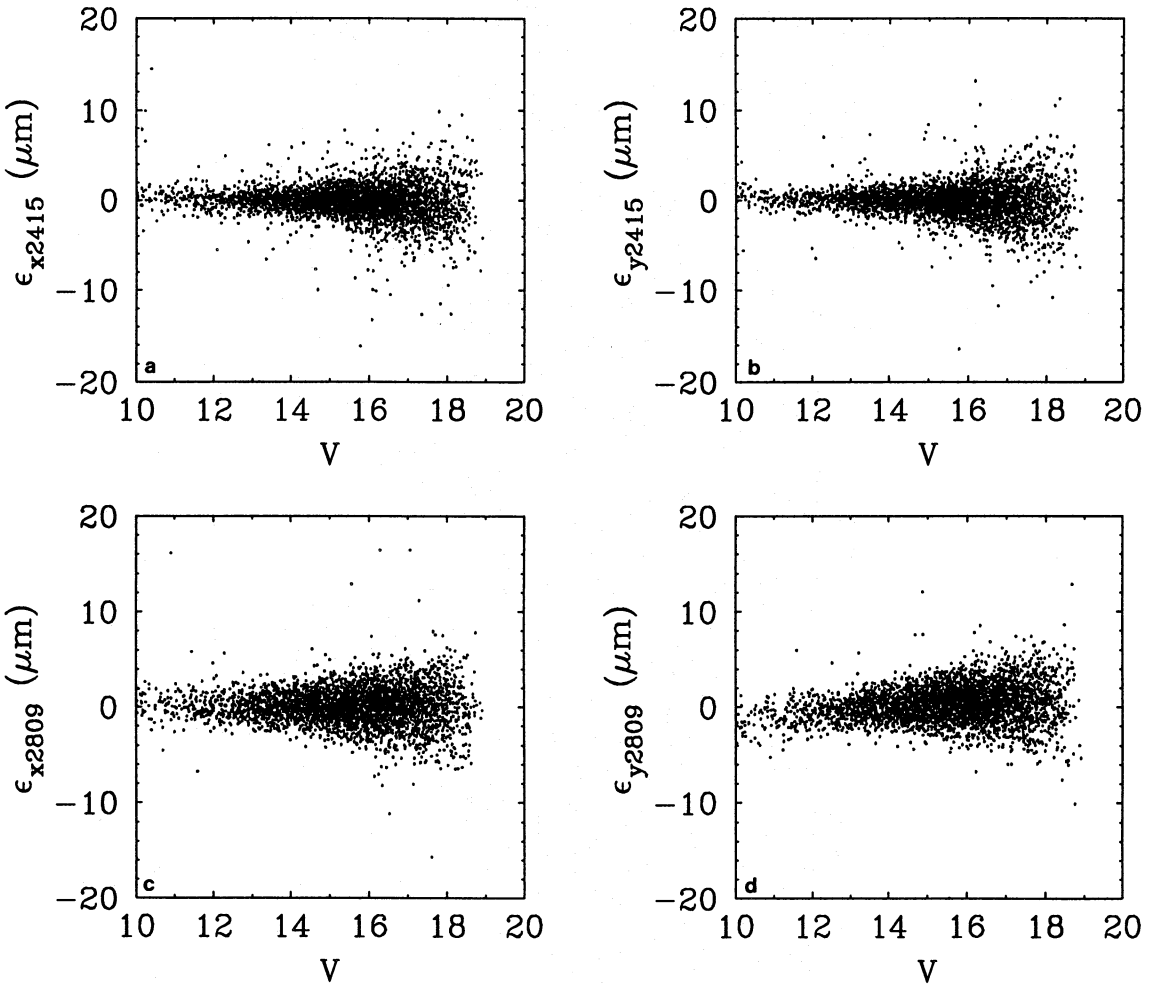

Fig. 7a–d. Residuals in microns in x and y coordinates as a function of V for T2415 and Cer 2809 plates. For the reference plate T2415 the dispersion mainly resulting from the centering methods. There is also no evidence for any significant magnitude effect

where non-biased estimations of σ_x and σ_y are taken as

$$\sigma_x^2 = \frac{1}{K-2}\sum_{k=1}^{K} w_k^x \epsilon_k^{x2} = \frac{1}{K-2}\sum w_k^x (X_0 - \mu^x t_k - X_k)^2$$

and

$$\sigma_y^2 = \frac{1}{K-2}\sum_{k=1}^{K} w_k^y \epsilon_k^{y2} = \frac{1}{K-2}\sum w_k^y (Y_0 - \mu^y t_k - Y_k)^2$$

Here ϵ_k^x and ϵ_k^y are the residuals in x and y coordinates on the plate.

$$\bar{t} = \frac{\sum w_k^x t_k}{\sum w_k^x}$$

or

$$\bar{t} = \frac{\sum w_k^y t_k}{\sum w_k^y}$$

Table 4. Accuracy in μm of centering methods in x and y coordinates as a function of magnitude for reference plate T2415.

V Mag interval	Number of stars	σ_{x2415} (in μm)	σ_{y2415} (in μm)
9.5-10.5	46	1.06	1.09
10.5-11.5	67	0.94	0.74
11.5-12.5	133	1.07	1.09
12.5-13.5	321	0.96	0.93
13.5-14.5	538	1.03	0.93
14.5-15.5	874	1.16	1.12
15.5-16.5	1206	1.50	1.45
16.5-17.5	1444	2.11	2.21
17.5-18.5	1383	2.30	2.35

4.4. Overall accuracy of the proper motion survey

The overall proper motion accuracy can be deduced from the various sources of errors. Sources of random errors are the plate noise, the digitizing machine, the centering algorithm, the plate to plate transform. Systematic errors are expected from the dif-

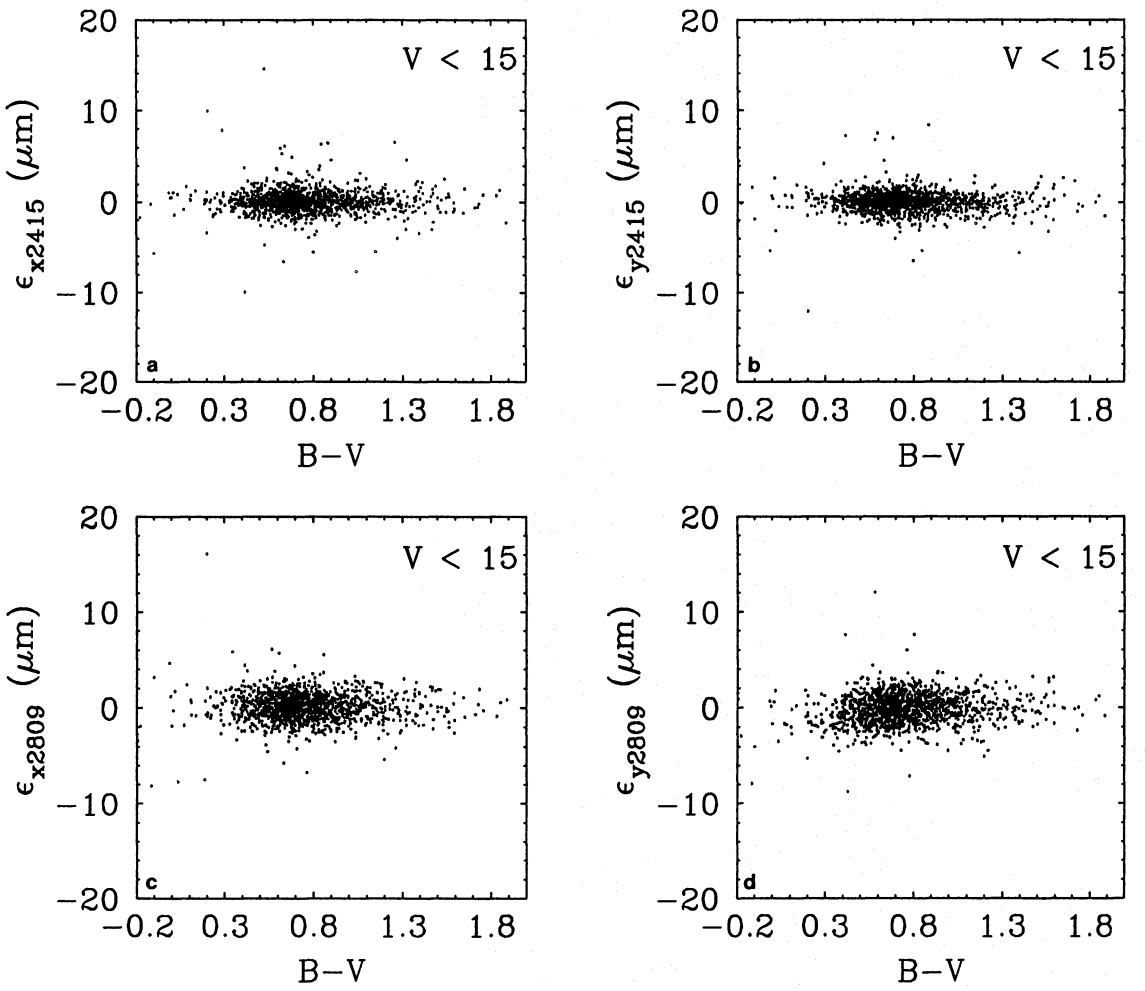

Fig. 8a–d. Residuals in microns in x and y coordinates as a functiom of (B-V) for T2415 and Cer2809 plates. There is no evidence for any significant color effect. Color term is found to be less than 0.34 μm

ferential atmospheric refraction which may create a color term in proper motion. To check the magnitude and color effects on proper motion, we have chosen two plates T2415 (B) and cer2809 (V). Figure 7a-d show the plots of residuals in x and y coordinates on two plates versus V magnitude and Fig. 8a-d show the plots of residuals versus (B-V) for stars V $<$ 15. As can be seen from Fig. 8a-d, the mean systematic errors in x and y is below 2 μm, and so negligible. From the Fig. 8a-d the color term in proper motion is found to be less than 0.34 μm per unit in B-V (slope: -0.21$\pm$0.13). So finally no correction has been applied. In the present survey, the overall accuracy turns out to be 0."25 per century for V$<$16 and 0."4 per century for V$>$17. The random error of the differential proper motions in arcsecond per century versus V magnitude diagram is shown in Fig. 9 and the mean error in differential proper motion (in arcsec per century) as a function of V magnitude is given in Table 5.

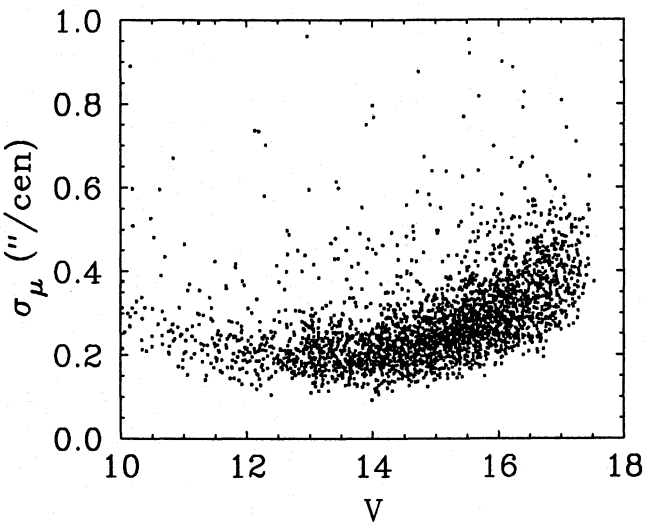

Fig. 9. The random error $\sigma_\mu = \sqrt{\sigma^2_{\mu^x} + \sigma^2_{\mu^y}}$ of the differential proper motions versus V magnitude

4.5. Reduction to absolute proper motion

The mean displacement of galaxies and quasars in the reference frame is used to calculate the zero point of the proper motion.

Table 5. The mean error (arcsec per century) in proper motion as a function of V magnitude

V mag interval	Number of stars	$<\sigma_\mu>$ ("/cen)
9.5-10.5	40	0.30
10.5-11.5	62	0.25
11.5-12.5	130	0.23
12.5-13.5	319	0.22
13.5-14.5	537	0.22
14.5-15.5	871	0.25
15.5-16.5	1200	0.32
16.5-17.5	1432	0.44

Most of the extragalactic objects have been visually verified in order to ensure that no unresolved multiple star or spurious image was misclassified as a galaxy. Some galaxies present a very large residual on the proper motion. They were indentified as oversized galaxies with extended structures. Such objects were eliminated and finally the mean proper motion of a sample of 377 galaxies and 9 quasars uniformly distributed throughout the ranges 11<V<18 and -0.8<(B-V)<1.8 has been used to calculate the absolute proper motion. The rms dispersion of galaxies and quasars motion is 0.80 arcseconds per century in μ_α and 0.71 arcseconds per century in μ_δ. The conversion equations are as follows:

$$\mu_\alpha(abs) = \mu_\alpha - 0.38 \pm 0.04(''/cen)$$

$$\mu_\delta(abs) = \mu_\delta - 0.43 \pm 0.04(''/cen)$$

5. Discussion

5.1. Comparison with other data

5.1.1. Photometry–comparison with GSPC stars

We have compared our photographic visual magnitudes (V_{Taut}) of 6 bright stars with the Guide Star Photometric Catalogue (GSPC) (Lasker et al. 1988). Lasker et al. have determined photoelectric magnitudes of 1477 stars in B and V band during the course of all sky survey. The comparison between the two measurements is shown in Table 6. Our photographic magnitudes and Lasker's photoelectric magnitudes for stars fainter than 10 are in good agreement within the error bars. For stars brighter than V=10 our calibration is not valid.

5.1.2. Astrometry–comparison with PPM stars

We have compared our results for high proper motion stars with the PPM stars (Röser & Bastian 1991). Table 7 indicates the differences in the two components of the relative proper motions. The agreement is good for bright stars considering the mean error bars in μ_α and μ_δ on the PPM measurements (0.2 to 0.5 arcsec/century).

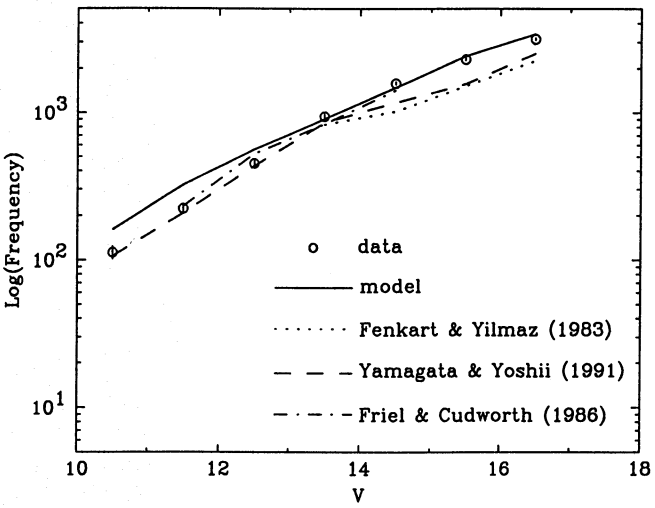

Fig. 10. Comparison of V star counts with other data sets and Besançon model prediction

5.2. Comparison with model predictions

Before comparison with Besançon model, it is important here to recall briefly the characteristics of the model. The model is described in detail by Robin & Crézé (1986), Bienaymé et al. (1987) and Robin & Oblak (1987). Table 8 shows the kinematical parameters used for the disk, thick disk and halo population for the model predictions. The disk is composed of 6 isothermal components in the model. The values of the solar motions are: U⊙=10.3 km s^{-1}, V⊙=6.3 km s^{-1} and W⊙=5.9 km s^{-1} in the model. A radial gradient in σ_U ($\partial ln\sigma_U^2/\partial r$) has been introduced in the model. This value is adopted from the estimation by Oblak & Mayor (1987) for F, G and K– type stars. The rotational velocity for the thick disk has been set to 173 km s^{-1} in the model, as a result from the analysis of our survey. The age-metallicity relation is adopted from Twarog (1980). The values of metallicity gradient (vertical and radial) for the three populations shown in the model, have been determined by comparing 5 data sets in different directions (Robin in preparation).

5.2.1. Star counts

Comparison of the observed star counts with model predictions is shown in Fig. 10 for 18.8 square degree field. The error bars are $\pm\sqrt{N}$, where N is the number of stars in each bin. In the same diagram we have compared data from Friel & Cudworth (1986) in the same direction but at opposite latitude ($l = 175°, b = -49°$), from Yamagata & Yoshii (1992) and from Fenkart & Esin-Yilmaz (1983) in SA54 direction ($l = 200°, b = 59°$). For 13≤V≤17, the observed and model predicted total counts for our survey agree well, though in the model we find more stars below V=13. For 11≤V≤15, there is a good agreement between Friel & Cudworth and our star counts. After V=14, Yamagata & Yoshii and Fenkart & Esin-Yilmaz star counts lie clearly below our counts, which can be explained by the difference in longitude and latitude between the two fields.

Table 6. Comparison of photographic magnitudes with GSPC photoelectric magnitudes

Stars	V_{GSPC}	V_{Taut}	$(B-V)_{GSPC}$	$(B-V)_{Taut}$
P166-A	9.47 ± 0.00	8.80 ± 0.05	0.62 ± 0.00	0.44 ± 0.06
P166-B	10.42 ± 0.03	10.21 ± 0.05	0.81 ± 0.00	0.88 ± 0.07
P166-D	13.11 ± 0.02	13.24 ± 0.06	0.49 ± 0.00	0.41 ± 0.07
P166-E	14.44 ± 0.03	14.47 ± 0.06	0.63 ± 0.02	0.60 ± 0.07
P166-F	14.89 ± 0.04	15.01 ± 0.06	0.67 ± 0.03	0.66 ± 0.07
P166-G	$15.62 \pm *$	15.63 ± 0.05	$0.72 \pm *$	0.72 ± 0.07

Table 7. Comparison with PPM high proper motion stars

PPM Number	μ_α Taut ("/cen)	$\mu_{\alpha err}$ Taut ("/cen)	μ_δ Taut ("/cen)	$\mu_{\delta err}$ Taut ("/cen)	$(\mu_{\alpha PPM} - \mu_{\alpha Taut})$ ("/cen)	$(\mu_{\delta PPM} - \mu_{\delta Taut})$ ("/cen)	Mag
32194	3.18	0.39	-2.51	0.23	0.18	0.01	10.5
32195	-0.63	0.29	-0.20	0.50	-0.71	-1.30	10.5
32242	-2.32	0.32	1.46	0.46	-0.91	-0.36	10.3
32248	-4.42	0.93	-1.98	0.53	0.58	0.18	8.6
32289	-2.94	0.60	0.91	0.59	-0.40	-0.71	8.5
32294	-0.16	0.23	0.40	0.24	-0.60	-0.30	11.0
32300	0.73	0.35	-1.48	0.31	-0.15	-0.62	10.5
51340	-6.41	0.89	1.28	0.92	1.24	1.52	7.5
51363	1.57	0.48	-6.38	0.95	-0.58	1.58	9.4
51364	-2.34	0.25	-3.43	0.39	-0.98	-0.17	10.0
51399	-2.09	0.17	-1.80	1.81	-1.15	0.80	10.6
51404	0.08	0.47	-0.24	0.37	-0.86	0.24	9.7
51471	-5.19	0.31	0.58	0.19	-0.68	0.42	10.2

Table 8. The characteristics of the Besançon model used for the comparison with real data

Disk	Age (in yrs)	σ_U km s^{-1}	σ_V km s^{-1}	σ_W km s^{-1}	Vrot km s^{-1}	[Fe/H]	$\frac{\partial[Fe/H]}{\partial z}$ dex kpc^{-1}	$\frac{\partial[Fe/H]}{\partial r}$ dex kpc^{-1}
	.15E9	16.7	10.8	6.0	-	0.01	-0.5	-0.07
	1E9	19.8	12.8	10.0	-	0.03	-0.5	-0.07
	2E9	27.2	17.6	13.0	-	0.03	-0.5	-0.07
	3E9	30.2	19.5	18.5	-	0.01	-0.5	-0.07
	5E9	34.5	22.2	20.0	-	-0.07	-0.5	-0.07
	7E9	34.5	22.2	20.0	-	-0.14	-0.5	-0.07
	10E9	34.5	22.2	20.0	-	-0.37	-0.5	-0.07
Thick disk	-	51.0	38.0	35.0	173	-0.7	0.0	-0.3
Halo	-	131.0	106.0	85.0	0	-1.7	0.0	0.0

5.2.2. Color distribution

(B-V) distributions (Fig. 11a-d) in different magnitude intervals have been compared with the model. Our (B-V) distribution presents a good agreement with the model over all the magnitude intervals. For 13≤V≤15, there is better agreement between Friel & Cudworth field and ours. The SA54 data from Yamagata & Yoshii and Fenkart & Esin-Yelmaz lie below our distribution as was already mentioned with the V star counts. The bump of red stars (1.0≤B-V≤1.5) which appears at the faintest magnitude corresponds mainly to late type disk dwarfs.

Comparison of (U-B) distribution is shown in Fig. 12a-d. The observed and model predicted counts agree well for all the magnitude ranges.

At V>16 the red stars are lost in the histogram because of B magnitude cut-offs. The observed starcount data are also presented in a tabular form in Table 9 for N(V,B-V) and in Table 10 for N(V,U-B). The dark line indicates the limit of reliability for starcount data.

5.2.3. Proper motion distribution

Figure 13a-d and 14a-d show the histograms of observed and model predicted proper motions in μ_l and μ_b respectively in four magnitude ranges. For doing model predictions, we assume that the proper motion error is a quadratic form of the magnitude, as measured in the real data. Due to the stellar drift, the asymmetric shape of the distribution of longitude proper motion is clearly visible in data and model. The observed proper motion distribu-

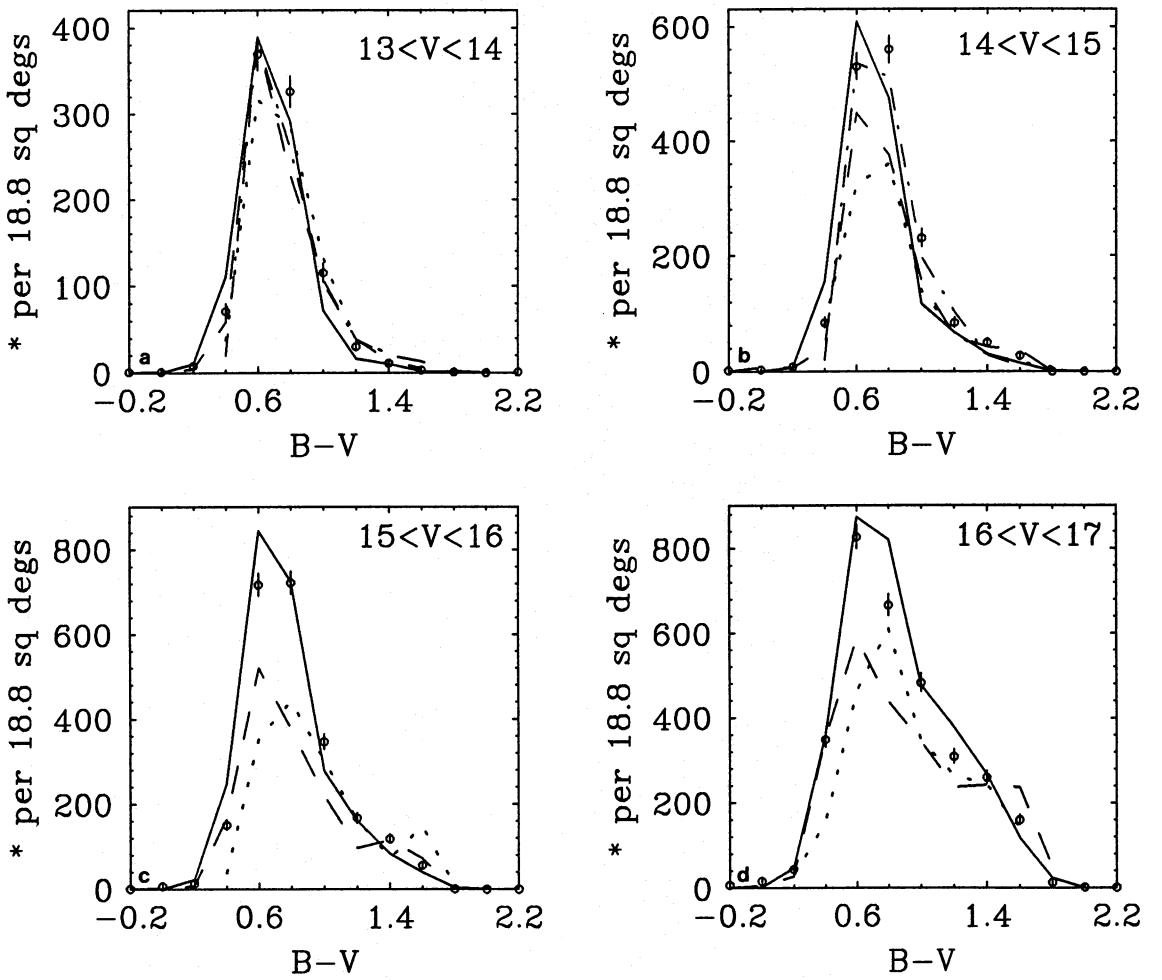

Fig. 11a–d. Comparison of the (B-V) distribution with other surveys and model prediction. The symbols are as in Fig. 10

Table 9. Starcounts over 18.8 square degrees as a function of V and B-V

B-V / V	-0.4	-0.2	0.0	0.2	0.4	0.6	0.8	1.0	1.2	1.4	1.6	1.8	2.0	2.2	Total
10.0-10.5	0	0	4	8	12	4	9	5	3	2	1	1	0	0	49
10.5-11.0	0	0	1	4	15	9	10	14	6	2	0	2	0	0	63
11.0-11.5	0	1	1	4	20	13	14	16	16	2	1	0	0	0	88
11.5-12.0	0	0	2	4	28	44	25	13	13	4	1	0	0	0	134
12.0-12.5	1	0	0	3	19	70	42	27	7	3	1	0	0	0	173
12.5-13.0	0	2	0	5	28	97	74	49	12	5	0	0	0	0	272
13.0-13.5	1	0	1	4	48	183	127	43	9	4	2	1	0	0	423
13.5-14.0	1	1	0	4	23	186	199	72	21	7	1	0	0	1	516
14.0-14.5	1	1	2	5	48	238	228	110	31	20	8	0	0	0	692
14.5-15.0	1	1	1	3	36	292	332	120	53	30	19	0	0	0	888
15.0-15.5	1	0	3	5	57	335	355	164	67	44	26	1	0	0	1058
15.5-16.0	3	1	4	8	93	382	367	182	100	74	30	0	0	0	1244
16.0-16.5	1	2	6	12	140	427	353	232	145	107	68	1	0	0	1494
16.5-17.0	6	5	10	32	208	399	313	250	163	152	92	12	2	1	1645

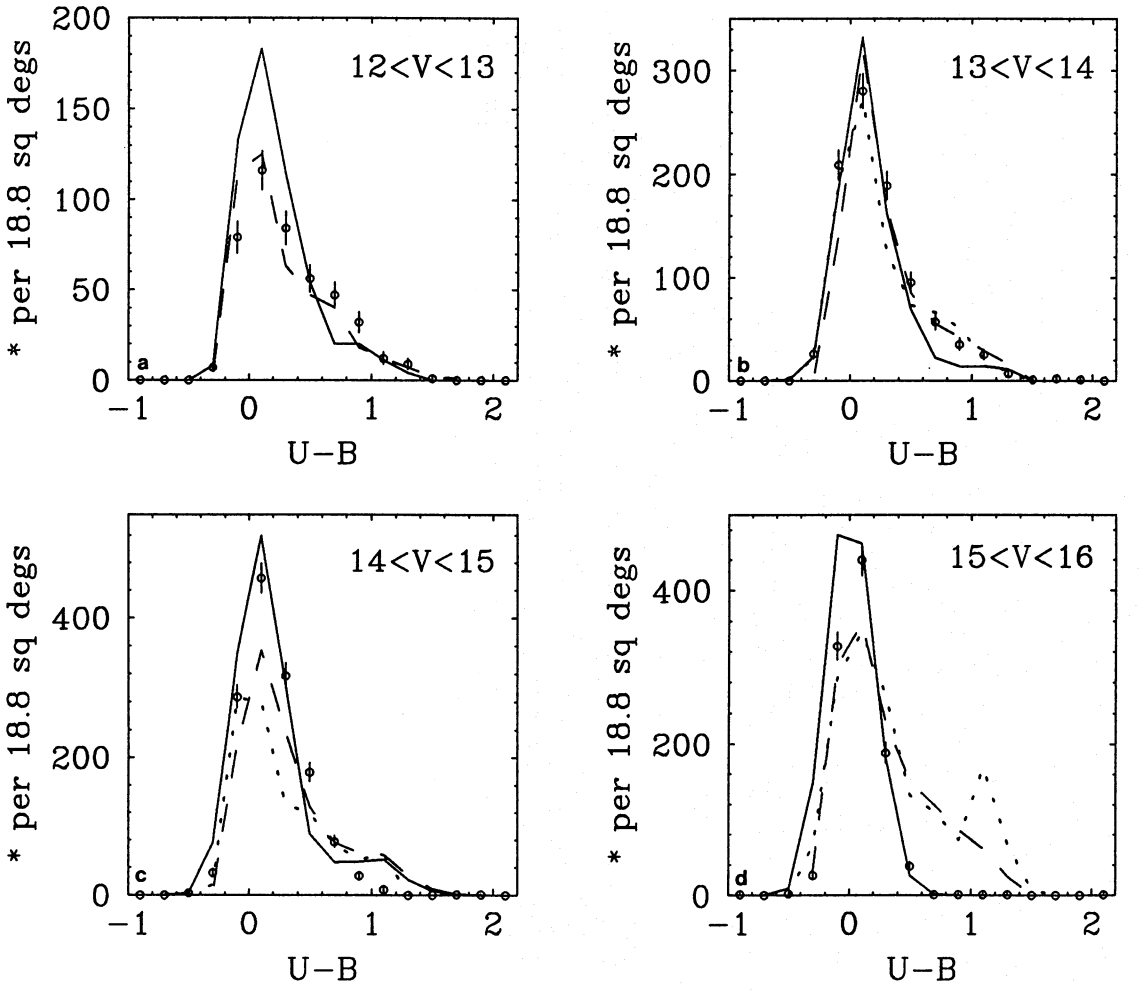

Fig. 12a–d. Comparison of the (U-B) distribution with other surveys and model prediction. The symbols are as in Fig. 10

Table 10. Starcounts over 18.8 square degrees as a function of V and U-B

U-B / V	-1.0	-0.8	-0.6	-0.4	-0.2	0.0	0.2	0.4	0.6	0.8	1.0	1.2	1.4	1.6	1.8	2.0	2.2	Total
10.0-10.5	0	0	0	0	2	8	9	7	4	3	6	3	1	4	0	1	0	48
10.5-11.0	0	0	0	0	1	11	14	5	8	9	6	3	1	2	1	0	2	63
11.0-11.5	0	0	0	0	3	14	17	10	7	15	11	5	2	2	1	0	0	87
11.5-12.0	0	0	0	0	6	30	31	21	16	7	8	3	7	2	0	0	0	131
12.0-12.5	0	0	0	0	15	33	53	20	26	11	7	5	2	0	0	0	0	172
12.5-13.0	0	0	0	0	23	62	66	41	35	23	11	6	4	0	0	0	0	271
13.0-13.5	0	0	0	1	51	133	120	46	30	14	12	6	2	1	0	0	1	417
13.5-14.0	0	0	0	1	55	136	126	93	49	18	22	7	2	1	1	0	0	511
14.0-14.5	0	0	0	4	73	184	166	114	50	35	9	4	0	0	1	1	1	642
14.5-15.0	0	0	0	2	58	231	234	136	58	23	5	1	0	0	0	0	0	748
15.0-15.5	0	0	0	2	70	257	236	88	16	1	1	0	0	0	0	1	0	672
15.5-16.0	1	0	0	4	81	189	73	6	0	0	0	1	0	0	0	0	0	355
16.0-16.5	0	0	0	3	16	15	1	0	0	0	0	0	0	0	0	0	0	35
16.5-17.0	0	1	0	1	0	0	0	0	0	0	0	0	0	0	0	0	0	2

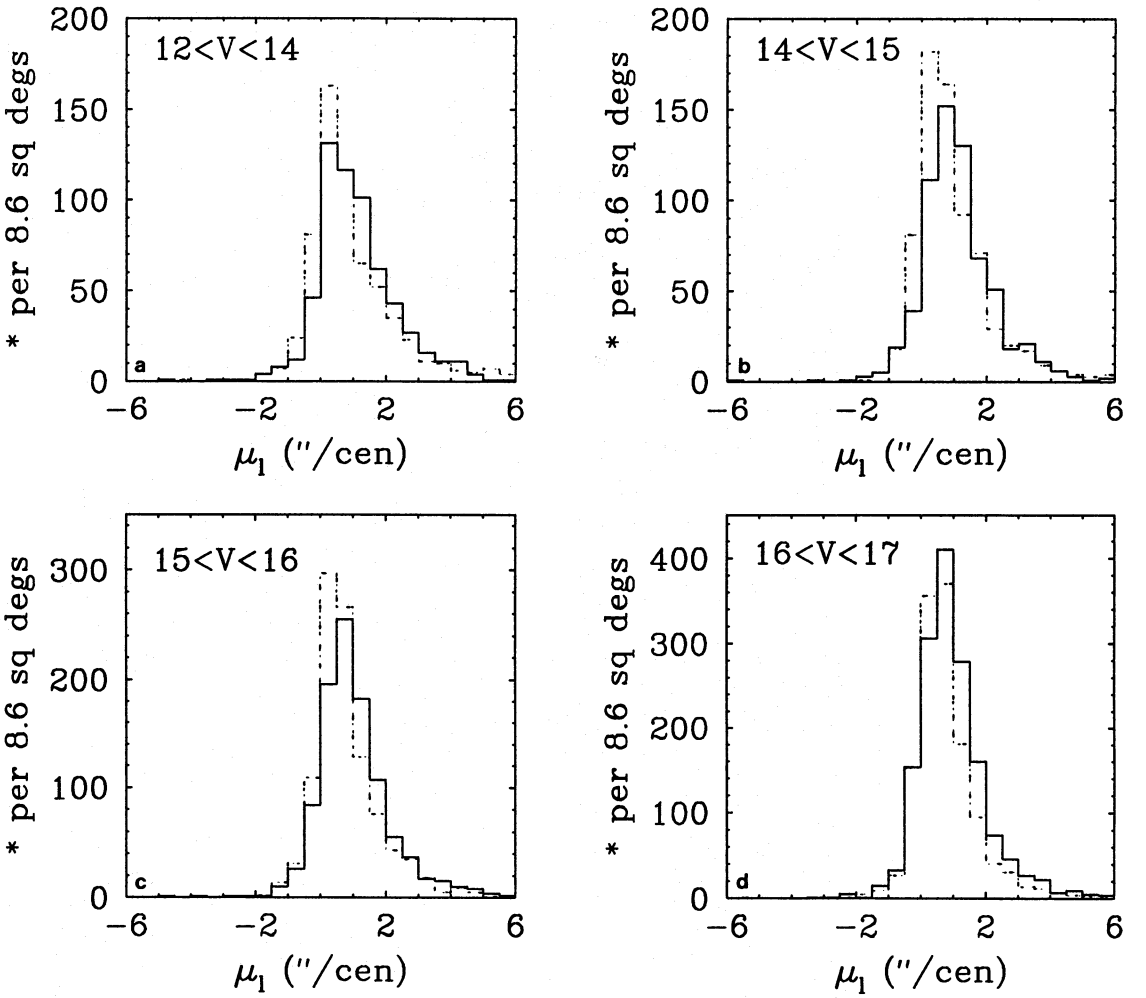

Fig. 13a–d. μ_l observed proper motion histograms for four magnitude intervals. Data (dash-dotted lines) and model prediction (solid lines)

tion (in μ_l and μ_b) agrees well for stars in the range 12<V<17 with the model.

5.3. Space motions

5.3.1. Distances

We have chosen a subsample of the stars in 0.3≤(B-V)≤0.9 color range (mainly F and G– type stars). The photometric distance of each star has been determined using a M_v and B-V relation. We assume as a conservative approach that the sample stars are all on the main sequence of the thin disk. But in our sample there exists also a proportion of giants and subgiants which is difficult to evaluate without spectra. When we compare our data with Besançon model predictions, we find that 8% of the stars in the sample are giants. Finally we decided to neglect this small contamination.

Another correction on distance concerns the variation of metallicity, which is partly due to the mixture of the thin disk, thick disk and halo stars whose mean metallicity is different. The local value of the vertical metallicity gradient ($\partial[Fe/H]/\partial z$) is not well determined. Current estimates cover most values from -0.2 kpc^{-1} to -1.0 kpc^{-1}. We assume a vertical metallicity gradient as in Kuijken & Gilmore (1989) :

$$\frac{\partial[Fe/H]}{\partial z} = \text{-0.3 kpc}^{-1}$$

which is a value found in recent determinations near the plane. To neglect such a gradient would lead to a systematic overestimate of the distances. However this approach does not allow to account for the thick disk specific metallicity which is probably a source of overestimation of the distance for these stars.

UV excess $\delta_{0.6}$ from the metallicity is calculated for each star according to Carney (1979) and the correction ΔM_v as a function of B-V and $\delta_{0.6}$ (Laird et al. 1988) is applied on distance measurements. In practice, a new distance is calculated, a revised ΔM_v correction applied, and so on up to convergence. The uncertainty on distance depends mainly on the photometric uncertainties and has been estimated to be $\sim$ 20 % in our case. However this uncertainty does not include the effects of metallicity, giants and subgiants fraction.

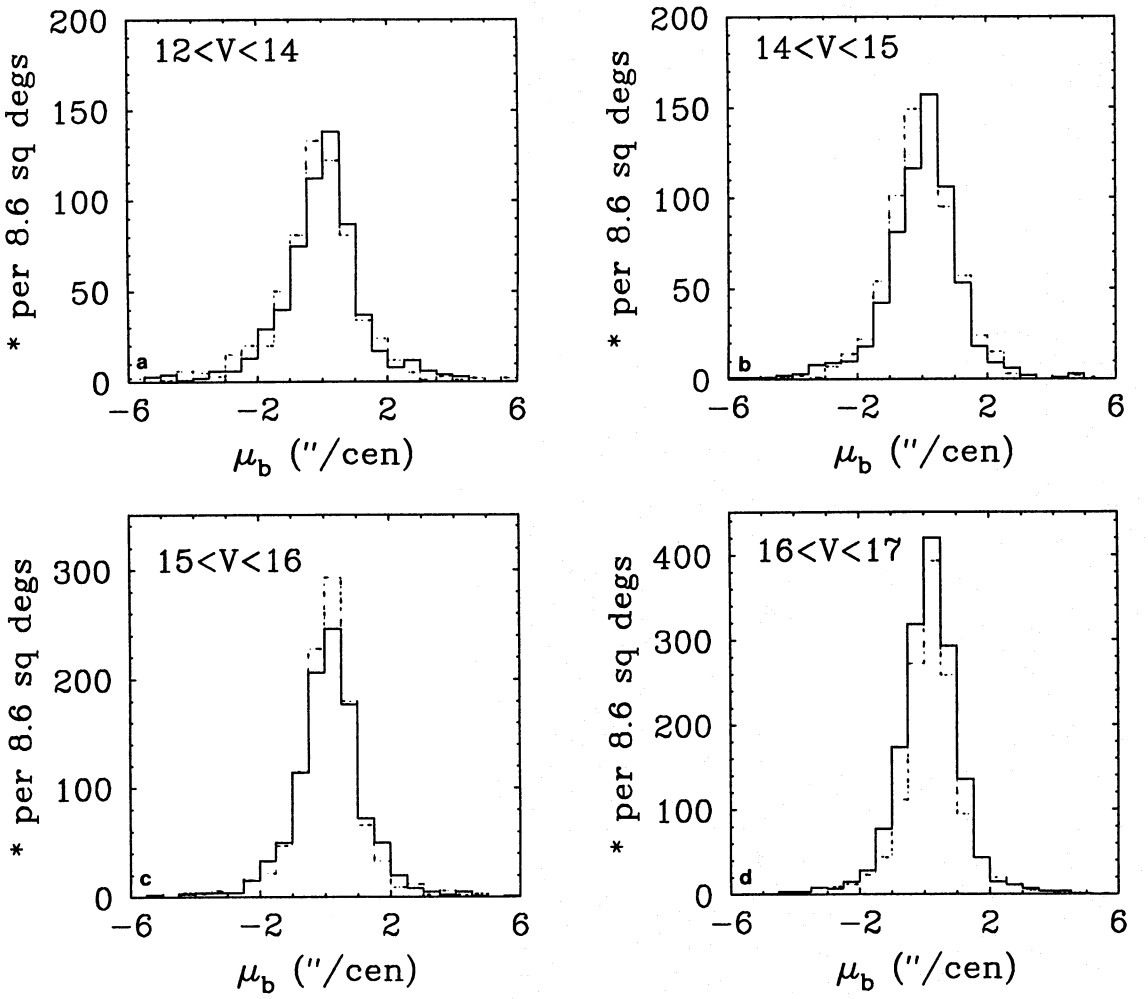

Fig. 14a–d. μ_b observed proper motion histograms for four magnitude intervals. Data (dash-dotted lines) and model prediction (solid lines)

5.3.2. Stellar space velocities

The measured proper motions have been directly converted to U+W and V velocities using the following relations:

$$U + W = 4.74.r.\mu_b \quad (\text{km s}^{-1})$$

$$V = 4.74.r.\mu_l \qquad (\text{km s}^{-1})$$

Where U,V & W denote the velocities in the galactic coordinate system relative to the Sun (opposite to the galactic centre, in the direction of galactic rotation and perpendicular to the galactic plane respectively), r is the distance (line of sight) of the star in pc and μ_l & μ_b are proper motions of the star ("/year) in l and b coordinates. The velocity error limit of our sample is $\sim$ 10 km s^{-1}kpc^{-1}. Figure 15a and b show the distribution of the computed stellar U+W and V velocities as a function of the estimated distances. Within 1 kpc, most of the stars are clustered between -50 and 50 km s^{-1} in U+W and there is a slow decrease in V velocity. This corresponds very well to the kinematical characteristics of the thin disk. Beyond 1 kpc, an asymmetric drift can be seen because of the growing contribution from higher velocity stars.

5.3.3. Radial gradient of the velocity dispersion

Bienaymé et al. (1992) have obtained similar data in a field towards galactic centre at intermediate latitude. The same method of determination of velocities has been applied to their data. Comparing the velocity dispersion in the two fields (Fig. 16a), we obtain a measure of the radial gradient of σ_{U+W} ($\frac{\partial ln\sigma^2_{U+W}}{\partial r}$) . The value is found to be -0.21$\pm$0.1 kpc^{-1}, which is in good agreement with the estimation (-0.2 kpc^{-1}) by Oblak and Mayor (1987) for F, G and K– type stars.

5.3.4. The nature of the old disk

By comparing the star count ratio between the two data sets in the 0.3$\leq$(B-V)$\leq$0.9 color bin (Fig. 16b), we deduce the scale length of the old disk which is found to be 2 to 2.5 kpc. This value is in close agreement with Mohan et al. (1988) value (2.5 kpc) obtained by Schmidt plate survey in the anticentre direction in

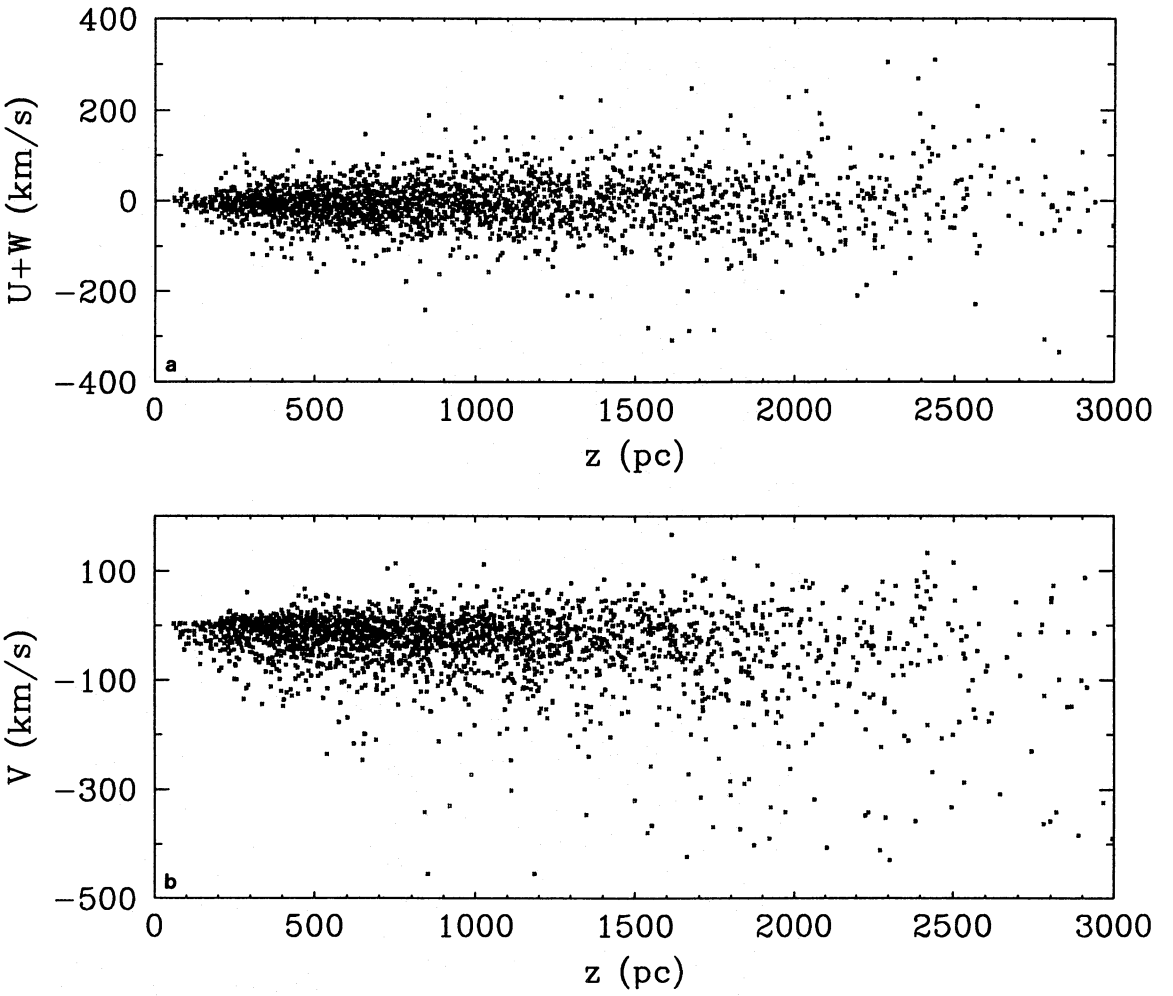

Fig. 15a and b. Distribution of U+W and V velocities versus the distance above the plane z(pc)

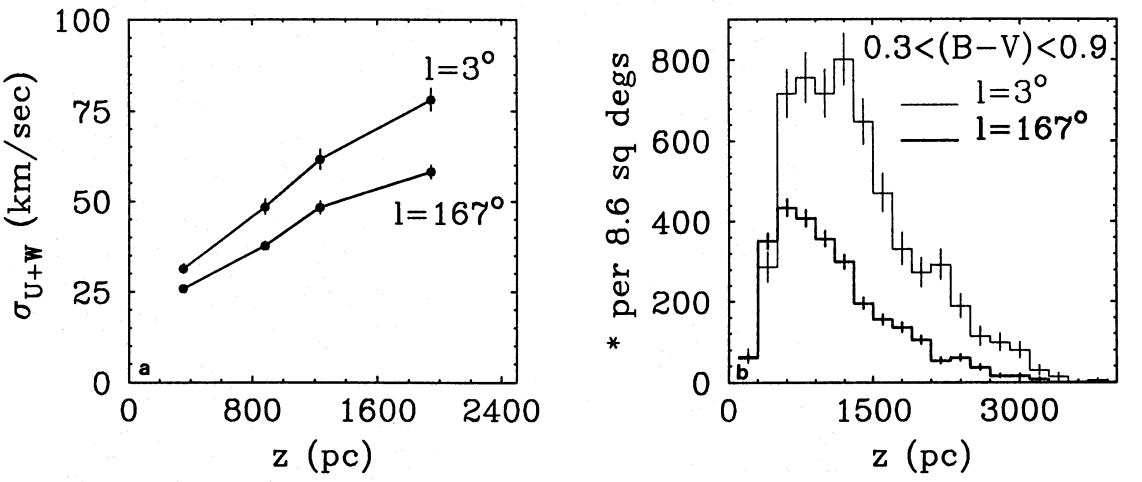

Fig. 16. a Plot of σ_{U+W} as a function of z distances for this survey (lower part) and for galactic centre field (upper part) (l = 3°, b = 47°) normalized to the same area. **b** Distribution of z distances for two data sets. Dark solid line corresponds to this survey and thin line corresponds to galactic centre direction

the galactic plane and recently confirmed by Robin et al. (1992) using much deeper CCD probes.

The algorithm SEM (Stochastic Estimation Maximization; Celeux & Diebolt 1986) is used for the deconvolution of multivariate gaussian distributions using a maximum likelihood criterion. Table 11 shows the kinematical parameters derived for the thin disk up to a distance z = 1750 pc. A vertical gradient is observed up to z = 1250 pc in the asymmetric drift and in σ_{U+W} and σ_V. In the four bins the parameters are in a good agreement, except in the last bin, which differ quite significantly from others. This effect is expected from the varying contribution of thin disk, thick disk and halo stars. The thin disk is in minority in this last bin. The mean velocities for this population are $(\overline{U+W},\overline{V})$ = (1±4,-14±2) km s^{-1} with velocity dispersions (σ_{U+W},σ_V) = (43±2,34±1) km s^{-1}.

5.3.5. The nature of the thick disk

Table 12 shows the kinematical parameters derived for the thick disk population. It is found that the thick disk has an asymmetric drift of 57±4 km s^{-1} with respect to LSR. This strengthens the hypothesis of a rapidly rotating population (V_{rot} = 173±4 km s^{-1}). This value is in close agreement with the recent results derived by Soubiran (1993) (179±16 km s^{-1}) for her NGP field.

The mean value of V velocity dispersion (σ_V) is 60±3 km s^{-1} for this population, which is similar to the value obtained by Ratnatunga & Freeman (1989) (54 km s^{-1}) and by Wyse & Gilmore (1986) (60 km s^{-1}).

The estimates of the halo parameters are less certain, because the error bars are larger and the halo population deconvolved in the farthest distance bin ($\bar{z}$ < 2000 pc) seems to be contaminated by disk stars. This may be due to the fact that our survey is not deep enough to contain much of this population.

In Fig. 17, the three gaussian populations representing the thin disk, the thick disk and the halo are overplotted on the V velocity histogram for the distance interval 1500<z<2500 pc.

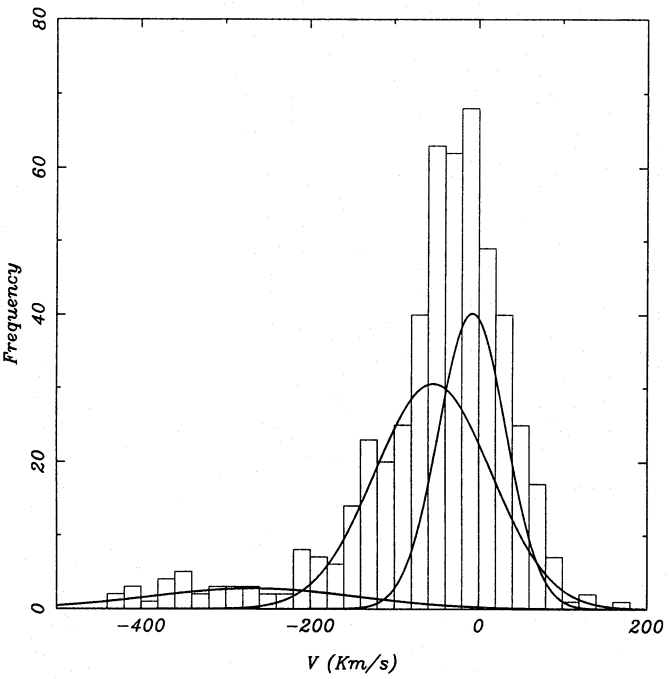

Fig. 17. Histogram of the V velocity for stars 1500<z<2500 pc. The 3 gaussian components solution of SEM corresponding to the thin disk, the thick disk and the halo are plotted

6. Conclusions

We have described a new complete survey of absolute stellar proper motions and multicolor photometry to V≤17 in the anticentre direction at intermediate galactic latitude. We characterize the data set, and discuss the data reduction methods used to produce accurate astrometry and photometry. The other data sets as well as model predictions are compared with the present survey in the overlapping magnitude ranges.

The result confirms that the disk has a relatively short scale length of 2 to 2.5 kpc. A radial gradient of velocity dispersion in U+W is found and we confirm an asymmetric drift of the order of 57 km s^{-1} and σ_V of 60 km s^{-1} for the thick disk population.

This investigation will be used together with data sets in several other directions in order to trace the velocity ellipsoid of the thick disk and the overall galactic structure.

Acknowledgements. This work forms a part of the PhD thesis of DKO, which was partially supported by the Indo-French Centre for the Pro-

Table 11. Results (km s^{-1}) of the SEM algorithm for the gaussian component corresponding to the thin disk in several bins of distance above the plane (pc). The standard errors on $< U+W >$, $< V >$, σ_{U+W} and σ_V are $\frac{\sigma_{U+W}}{\sqrt{N}}$, $\frac{\sigma_V}{\sqrt{N}}$, $\frac{\sigma_{U+W}}{\sqrt{2N}}$ and $\frac{\sigma_V}{\sqrt{2N}}$ respectively

z(pc)	0-700	700-1000	1000-1500	1500-1750
Ntot	1091	611	414	258
p(%)	80±3	86±3	76±14	45±9
Ndisk	873	525	315	116
$< U+W >$	-7±1	-5±2	-7±3	13±5
$< V >$	-11±1	-16±1	-17±2	-10±3
σ_{U+W}	26±1	36±1	44±2	48±3
σ_V	21±1	31±1	37±1	35±2

Table 12. Same as Table 11, for the thick disk

z(pc)	0-700	700-1500	1500-2500	2500-3500
Ntot	1091	1025	508	61
p(%)	20±0.2	25±1	52±8	70±0.4
Nthdisk	218	256	264	43
$< U+W >$	-17±4	-1±4	-2±4	2±10
$< V >$	-56±4	-60±4	-54±4	-44±12
σ_{U+W}	53±3	69±2	68±3	64±7
σ_V	53±3	61±3	68±3	80±9

motion of Advanced Research / Centre Franco-Indien Pour la Promotion de la Recherche Avancée, New-Delhi. We thank Dr. Michel Crézé for his critical reading of the manuscript, and for useful suggestions that have resulted in a significant improvement in the presentation. The authors would like to thank Dr. Elena Schilbach for fruitful discussions which occurred during this work. We especially thank the referee Dr. Gerry Gilmore for his comments. We also thank all the MAMA, OCA and Tautenburg Schmidt staffs who made this investigation possible.

References

Bahcall J. N., Soneira R. M., 1981, ApJS 44, 73
Berger J., Cordoni J. P., Fringant A. M., et al., 1991, A&AS 87, 389
Bienaymé O., Robin A. C., Crézé M., 1987, A&A 180,94
Bienaymé O., Mohan V., Crézé M., et al., 1992, A&A 253, 389
Bienaymé O., 1993, A&A (in press)
Carney B.W., 1979, ApJ 233,211
Celeux G., Diebolt., 1986, Rev. Statistique Appliquée, 34, 35
Chareton M., Considère S., Bienaymé O., 1993, A&AS (in press)
Chiu L. T. G., 1980, ApJS 44, 31
Fenkart R., Esin-Yilmaz F., 1983, A&AS 54, 423
Friel E.D., Cudworth, K.M., 1986, AJ 91, 293
Gilmore G., Wyse R. F. G., 1985, AJ 90, 2015
Guibert J., 1983, Bull. Inform. CDS 25, 13
Kuijken K., Gilmore G., 1989, MNRAS 239, 605
Laird J.B., Carney B.W., Latham D.W., 1988, AJ 95, 1843
Lasker B.M., Sturch C.R., Lopez C., et al., 1988, ApJS 68, 1
Majewski S. R., 1992 , ApJS 78, 87
Mohan V., Crézé M., 1987, A&AS 68, 529
Mohan V., Bijaoui A., Crézé M., et al., 1988, A&AS 73, 85
Mohan V., Ojha D.K., Bienaymé O., et al., 1993, JA&A (in preparation)
Notni P., Börngen F., Ziener R., 1979, Astron. Nachr. 300, 287
Oblak E., Mayor M., 1987, Evolution of Galaxies, X IAU European Meeting, J.Palous (ed.), Publ. Astro. Inst. Czech. Acad. Sci. 69, 263
Pelat D., 1988 , Traitement De L'Informations - Méthodes et Concepts, Benest D. (ed), Comptes rendus de l'ecole de Goutelas, France, p. 11
Ratnatunga K.U., Freeman K.C., 1989, ApJ 339, 126
Reid N., 1990, MNRAS 247, 70
Reid N., Majewski S.R., 1993, ApJ 409, 635 1993
Robin A. C., Crézé M., 1986, A&A 157, 71
Robin A. C., Oblak E., 1987, Publ. Astron. Inst. Czech. Acad. Sci. 69, 323
Robin A.C., Crézé M., Mohan V., 1992, A&A 265,32
Robin A. C. (in preparation)
Röser S., Bastian U., 1991, PPM Star Catalogue, Astronomisches Rechen-Institut Heidelberg; Spektrum, Akad. Verl.
Schilbach E., 1993, (private communication)
Soubiran C., 1992a, A&A 259, 394
Soubiran C., 1992b, Thèse de Doctorat de l'Observatoire de Paris
Soubiran C., 1993, A&A 274, 181
Spaenhauer A., 1989, The Gravitational Force Perpendicular to the Galactic Plane. Philip A. G . D., Lu P. K. (eds.) Proc of a Conference held at Danbury. David Press, Schenectady,N. Y., P.45
Twarog B.A., 1980, ApJ 242, 242
Wyse R.F.G., Gilmore G., 1986, AJ 91, 855
Yamagata T., Yoshii Y., 1992, AJ 103, 117

This article was processed by the author using Springer-Verlag LaTeX A&A style file version 3.